

First principles calculation of structural, electronic and optical properties of (001) and (110) growth axis (InN)/(GaN)_n superlattices

B. Bachir Bouiadjra^a, N. Mehnane^{a,*}, and N. Oukli^b

^a*Applied Materials Laboratory (A.M.L), Faculté de Genie Electrique, University Djillali Liabes of Sidi Bel Abbes, 2200 Sidi Bel Abbes Algeria.*

^b*Laboratory of Macromolecular and Physical Organic Chemistry (LCOPM), Faculty of Sciences, University Djillali Liabès, 22000 Sidi Bel Abbès, Algeria.*

Received 21 June 2020; accepted 7 October 2020

Based on the full potential linear muffin-tin orbitals (FP-LMTO) calculation within density functional theory, we systematically investigate the electronic and optical properties of (100) and (110)-oriented (InN)/(GaN)_n zinc-blende superlattice with one InN monolayer and with different numbers of GaN monolayers. Specifically, the electronic band structure calculations and their related features, like the absorption coefficient and refractive index of these systems are computed over a wide photon energy scale up to 20 eV. The effect of periodicity layer numbers *n* on the band gaps and the optical activity of (InN)/(GaN)_n *SL_s* in both growth axis (001) and (110) are examined and compared. Because of prospective optical aspects of (InN)/(GaN)_n such as light-emitting applications, this theoretical study can help the experimental measurements.

Keywords: Gallium nitride; growth axis; InN/GaN superlattices; optical properties.

PACS: 71.20.Nr; 71.55.Eq; 73.21.Cd; 73.21.Fg

DOI: <https://doi.org/10.31349/RevMexFis.67.7>

1. Introduction

The group III-nitride semiconductors have aroused the interest of experimenters as well as theoreticians [1, 29], such as Gallium nitride and indium nitride and their solid solutions are III-V semiconductor that gained significant attention for constructing multi Quantum well based optoelectronic devices: laser diodes and light-emitting diodes [5]. To optimize and exploit the potential of the GaN and InN for further optoelectronics applications and solar cell technology, superlattices (*SL_s*) are one of the simplest ways to tailor the electronic and optical properties of the materials. Especially, it has been shown that *SL_s* systems can be very useful for theoretical investigation. The cause for that is that atomic monolayers of GaN and InN in InN/GaN *SL_s* are grown separately and with the wanted width for each layer. It is found in literature many studies showing InN/GaN system make the design of various InN-based heterostructure devices possible [6, 11]. Indeed, its bandgap can cover the whole solar spectrum solely by changing the number of GaN monolayers in InN/GaN *SL_s* [12, 15]. It is well known that crystal orientations have a significant impact on their properties and their potential applications. They can be generated artificially during the growth process, but they can also occur naturally since a change of orientation can be induced by temperature or pressure [16, 18].

For lattice-matched heterostructures, the [110] orientation is particularly simple to handle (zinc-blende-type crystals) since the interface is nonpolar. For strained-layer *SL_s*'s, on the other hand, a theoretical description becomes substantially complicated because the atoms do not necessarily stay in planes perpendicular to the growth direction. The interface can then become polar [20]. Therefore, one expects qualita-

tive differences between the energetics of (110) growth and growth in all other orientations [20]. In recent years, there has been some experimental [21, 24] and lots of theoretical research [25, 28] conducted on the physical properties of III-compounds *SL_s*, oriented along the (110). I. Gorczyca *et al.* [29] have investigated the electronic structures of the composition InN/GaN by comparing three different orientations of the growth direction in wurtzite phase by using the self-consistent *ab initio* calculations based on the density functional theory (DFT). I. Gorczyca *et al.* [8] have investigated the bandgap behavior based on first-principles calculations of electronic band structures for various short period nitride *SL_s*. It is shown that for *SL_s*, it is possible to exceed by far the range of band gap values, which can be realized in ternary alloys. G. Staszczak *et al.* [30] studied the measurements of photoluminescence and its dependence on hydrostatic pressure, which are performed on a set of InN/nGaN *SL_s* along the growth axis (001), with one InN monolayer and with different numbers of GaN monolayers. It has been found that the transition energies for *SL_s* are significantly higher than the calculated band gaps for the same kind of *SL_s*. However, to our knowledge, the (InN)_{*m*}/(GaN)_{*n*} *SL_s*'s with various growth axis directions have been given less or no attention. Our aim here is to investigate the symmetry of (110)-oriented *SL_s* but also to give all the details concerning the (001) symmetries. The goal is to be able to predict the detailed electronic and optical characteristics of *SL_s* grown along (001) and (110) direction using first principles calculations whose is devoid of adjustable parameters and can help shed light on different aspects of the problem. The paper is structured as follows. The computational method we have adopted for the calculations is briefly described in Sec. 2. The

most relevant results obtained are presented and discussed in Sec. 3. Finally, in Sec. 4, we summarize the main conclusions of this work.

2. Detail of calculation

In the present study, the structural and electronic properties of binary InN and GaN compounds and their $(\text{InN})_m/(\text{GaN})_n$ superlattices are investigated using the first-principles full potential linear muffin-tin orbitals method (FP-LMTO) [31] simulation program based on the density functional theory (DFT) within generalized gradient approximation (GGA96) [32] using the parameterization of Perdew *et al.* [33]. The space in the (FP-LMTO) method is divided into non-overlapping muffin-tin (MT) spheres centered at the atomic sites separated by an interstitial region (IR). In IR, the s, p and d basis functions are expanded in a number (NPLW) of plane waves, hence treating the interstitial regions on the same footing as the core regions. Inside the (MT) spheres, the basis sets are described by radial solutions of the one-particle Schrödinger equation (at fixed energy) and their energy derivatives multiplied by spherical harmonics. Both LMTO basis set and charge density are expanded in spherical harmonics up to $l_{\max} = 6$ (l_{\max} being the maximal angular momentum). The self-consistent calculations are considered to be converged when the total energy of the system in stable within 10^{-4} Ry.

Our aim here is to investigate the symmetry of (110)-oriented SL_s but also to give all the details concerning the (001) symmetry. We have then selected a series of $(\text{InN})_m/(\text{GaN})_n$ SL_s where $n = 1, 3, 5, 7$ and $m = 1$ (*i.e.*; the total number of monolayers varies from 2 to 8). We restrict ourselves to the case for which $(m + n)$ is even. The purpose here is to predict the detailed electronic and bonding properties of the titled systems by using first-principles calculations. Both (001) and (110) oriented SL_s , which were simulated in our study, have a tetragonal symmetry, m and n being the number of monolayers of InN and GaN, respectively. In Fig. 1, we show the direct lattice of a (001) and (110) growth axis made up of an alternation of one monolayer of InN and others of GaN. The set of primitive translation vectors of (001) and (110)-oriented SL_s are given by:

$$\begin{aligned} a_{x(001)} &= \frac{a_0}{2}[1, 1, 0]; & a_{y(001)} &= \frac{a_0}{2}[-1, 1, 0]; \\ a_{z(001)} &= a_0[0, 0, L] \end{aligned} \quad (1)$$

$$\begin{aligned} a_{x(110)} &= \frac{a_0}{2}[1, -1, 0]; & a_{y(110)} &= \frac{a_0}{2}[L, L, 0] \\ a_{z(110)} &= a_0[0, 0, 1] \end{aligned} \quad (2)$$

Here, the value of a_0 is a lattice constant of bulk materials, with $L = (m + n)/2$. The volume of the (001) and (110) SL_s direct primitive unit cell is $V_{(001)} = V_{(110)} = L \cdot a_0^3/2$, and there are $4L = 2(m + n)$ atoms per unit cell: m atoms of In, n atoms of Ga, and $(m + n)$ atoms of N. The symmetry of zincblende (ZB) InN/GaN SL_s grown along with the symmetry

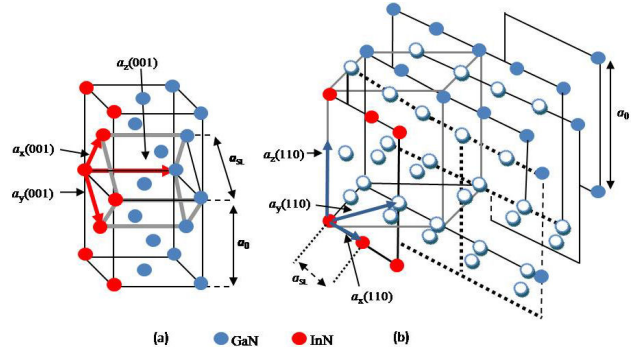


FIGURE 1. The direct zones of both bulk semiconductor and a (001) and (110) growth axis SL_s , with one InN monolayer and with different numbers of GaN monolayers. The set of primitive translation vectors a_x, a_y and a_z of the SL_s are also shown in this figure. a_0 and a_{SL} are the lattice constants of the bulk and the superlattice, respectively. a) (001) growth axis SL_s and b) (110) growth axis SL_s

axis depends on the numbers of monolayers m and n . We only focus on tetragonal symmetry. This procedure provides us with the desired space group of the SL_s structure when $m + n$ is even (this is the only case taken into consideration in the following our work). The appropriate space groups are D_{2d}^5 in both (001) and (110) growth axis SL_s if $m = n = 1$. However, when we choose the (110) as the axis of growth and for odd values of m and n , the group space is C_{2v}^1 .

3. Results and discussion

3.1. Structural properties

The Study of confinement effects and electronic structures in SL_s $(\text{InN})_m/(\text{GaN})_n$ along the (001) growth axes has been considerably focused over the past decade, but the most interesting feature is to know the effect of crystal orientations on their properties and their potential applications [34]. There is a wide variety of the growth axes enabling the realization of the SL_s . Two cases will be used: SL_s grown along with the (001) and (110) directions. While the structural properties of (001)-oriented semiconductor SL_s have been studied in great detail by using first-principles methods, there is not a comparable amount of information about the properties of (110)-oriented SL_s [12]. It is reported that (110) oriented SL_s exhibit considerably different characteristics compared to those grown along the (001) direction. We theoretically calculated these variations on ideal cases and to verify the expectation that their properties represent. The calculations in this work are carried out on ideal cases in which all atoms of the bulks or SL_s are located in ideal positions. By choosing the SL_s which have a short period, we can assume that the lattice parameter is constant throughout the crystal as the distance between the successive interfaces is very small. This approximation liberates us from any calculation of relaxation. For the considered structures, we perform the structural optimization by minimizing the total energy with respect to the cell parameters and also the atomic positions.

TABLE I. Calculated lattice parameter a_0 and bulk modulus B for the binary compounds InN and GaN at equilibrium volume compared to the available theoretical and experimental data.

	Lattice constant a_0 (Å)		
	Present	Expt.	Theoretical studies
InN	4.940	4.98[36]	4.947[8], 4.98[38], 4.995[39], 5.05[40]
GaN	4.480	4.50[43]	4.556[44], 4.46[45], 4.48 [46]
Bulk modulus B (GPa)			
	Present	Expt.	Theoretical studies
InN	141.23	137[41]	140.76 [8], 146[42]
GaN	192.564	190[47]	190.932[48], 172.2[49] 206.9[50]

For the binary compounds, the simplest structure is an eight-atom simple cubic cell. For both directions (001) and (110)-oriented SL_s , the smallest ordered structure is a four-atom tetragonal cell, corresponding to the SL(1,1) and the largest ordered structure is a sixteen-atom tetragonal cell, corresponding to the SL(1,7). The calculated total energies at many different volumes around equilibrium were fitted by the Murnaghan equation of state [35] in order to obtain the equilibrium lattice constant a_0 and the bulk modulus B for the binary compounds and all SL_s . It should be noted that the period of our SL_s is $D = L \times a_{SL}$, a_{SL} being the equilibrium lattice constant of the SL_s in the x direction. The lattice mismatch is found to be 9.76% for InN/GaN. Therefore, it may be crucial for SL systems. The results for the binary compounds are presented in Table I. As shown in Table I, the obtained results in our calculations are well compatible with other previous experimental and theoretical works for both binary compounds InN and GaN. The calculated equilibrium lattice parameters of our binaries InN and GaN in ZB structure are (4.940 Å) and (4.480Å), which differ by only

0.80% and 0.69% compared with the experimental results of 4.98Å [36] for InN and 4.5Å [35] for GaN, respectively. The calculated equilibrium lattice parameters of ZB-GaN is 4.480Å, which differ by only 0.69% of the experimental values of 4.50Å [42]. The calculated bulk modulus B for ZB InN and GaN shows good agreement with experimental results and previous theoretical studies and it is evident that GaN is less compressible than InN because Ga-N is more tightly bound than In-N and results in a higher covalence for Ga-N than for In-N [37].

The lattice constant and bulk modulus for (InN)/(GaN) $_n$ for different values of n in both directions (001) and (110)-oriented SL_s were calculated and are listed in Table II. As expected, the calculations for the (001) and (110) SL(1,1) give the same results since the symmetry is the same. The link between the bulk and the SL direct lattices is shown in the Fig. 1 with $a_x = a_y = a_{SL} = a_0/\sqrt{2}$ and $a_z = L \cdot a_0$ in (001) case ($a_{SL} = a_x = a_0/\sqrt{2}$, $a_y = L \cdot a_x$ and $a_z = \sqrt{2} \cdot a_x$ in (110) case). In the first-principles structural calculations, we can also try to obtain this a_z/a_x and a_y/a_x ratio by minimization. It is found from Table II that the lattice constant in all SL_s increases when a few percent of indium atoms is added to the host semiconductor GaN. If we take the case of a (001) and (110) (1.7) SL_s as an example, the host material is GaN with a lattice parameter of 4.48 Å. The incorporation of one InN monolayer increases the lattice parameter to a value of 4.640 and 4.651 Å, respectively. The increase in the lattice parameter is justified by the fact that the atomic size of indium is larger than those of Ga atom.

It is very clear from Table I that the bulk modulus for the (InN)/(GaN) $_n$ in both directions SL_s increases with the enhancement of the number of monolayer n , which suggests the same increasing for the compressibility of each compound. These compounds became harder when the number of monolayers n increase. It represents bond strengthening or weakening effects induced by changing the composition. The stability of (InN)/(GaN) $_n$ SL_s is examined by calculating their formation energies. The formation energy per atom E_{form}

TABLE II. The structural parameters of superlattices (InN)/(GaN) $_n$. Formation energies per atom are also listed. a_0 represents the lattice constant and B the bulk modulus for the SL_s . In the case of SL , a_0 is shown in Fig. 1 and the link with the SL lattice parameter is obvious: $a_{0,SL} = a_0/\sqrt{2}$.

Compounds	(001)-oriented Superlattice				
	a_0 (Å)	$a_{0,SL}$	c_0/a_0	B(GPa)	E_{form} (eV)
InN/GaN ₁	4.854	3.433	1.414	127.836	-0.0074
InN/GaN ₃	4.712	3.332	2.828	146.225	-0.0072
InN/GaN ₅	4.685	3.313	4.243	214.630	-0.0057
InN/GaN ₇	4.640	3.281	5.657	310.397	-0.0048
(110)-oriented Superlattice					
InN/GaN ₁	-	-	-	-	-
InN/GaN ₃	4.728	3.343	1.414	146.666	-0.0097
InN/GaN ₅	4.658	3.294	1.414	210.661	-0.0082
InN/GaN ₇	4.651	3.289	1.414	306.866	-0.0075

as a function of the number of monolayers n for all superlattices is calculated as follows [51]:

$$E_{\text{Form}} = E_{\text{tot}}^{(\text{InN}/\text{GaN})} - (E_{\text{tot}}^{\text{InN}} + E_{\text{tot}}^{\text{GaN}})/2 \cdot (n + 1), \quad (3)$$

where E_{tot} is the total energy of the $(\text{InN})/(\text{GaN})_n$ and the total energy of its constituent parts GaN and InN. From Table II analysis, it can be found that formation energy for these SL_s have negative values and decrease by a small amount with the number of monolayers. The sign of the formation energy indicates that the present systems are energetically more stable with increasing n and imply that these SL_s are exothermic and also can be synthesized experimentally. The (001) SL_s have formation energy slightly less than the formation energy of (110) SL_s .

3.2. Electronic structure and density of states

In this section, we turn our attention to study the electronic properties of the parents InN and GaN binary compounds and their SL_s via calculating the energy band structure by using our calculated values of the lattice parameter. The results exhibit that cubic GaN and InN are a direct bandgap, where the valence band (VB) maximum and conduction band (CB) minimum are found at the Γ point. The results clearly exhibit that the present calculated bandgaps of 0 eV for InN and 1.916 eV for GaN are, on the whole, underestimated compared to the experimental values of 0.7 eV for InN [52] and 3.20 eV for GaN [53], but are in right agreement with other theoretical studies. The large difference in the calculated values of the band gaps as compared to the experimental values can be explained by the well-known fact that, in the electronic band structure calculations within DFT, GGA underestimates the energy gaps in semiconductors, but this will not alter the conclusions of the present work since they are not related to the quantitative estimation of gaps.

The calculated band gap energies of $(\text{InN})/(\text{GaN})_n$ in both (001) and (110) directions as a function of the thickness of the monolayer GaN are investigated and plotted. As an example we show Fig. 2 the band structure of two limit configurations ($n = 1$ and $n = 7$), where E_f represents the Fermi level. From the results of the calculated bandgap energies, we find that these materials have a direct bandgap, both valence band maximum and conduction band minimum are lying at Γ point, which is of interest for optoelectronic devices. The symmetry points in Fig. 2 refers to the tetragonal Brillouin zone (BZ) are ($X, M, \Gamma, Z, A, \text{ and } R$) in (001) direction case and those in (110) direction case are ($X, M, Y, \Gamma, Z, A, R, \text{ and } B$). In the case of (001) $SL(1,1)$ the high symmetry points B and Y are identical to R and X , respectively. This remark remains valid for the (110) $SL(1,1)$, but B becomes different from R and Y from X when n increase. It is noticeably indicated that the empty bandgap at the zone center is moved down for these SL_s for the bulk GaN band structure (not presented here). We also notice significant changes in the CB behaviour near $R, A, Y,$ and Z for (110) compared with (001). When n increase, the bottom

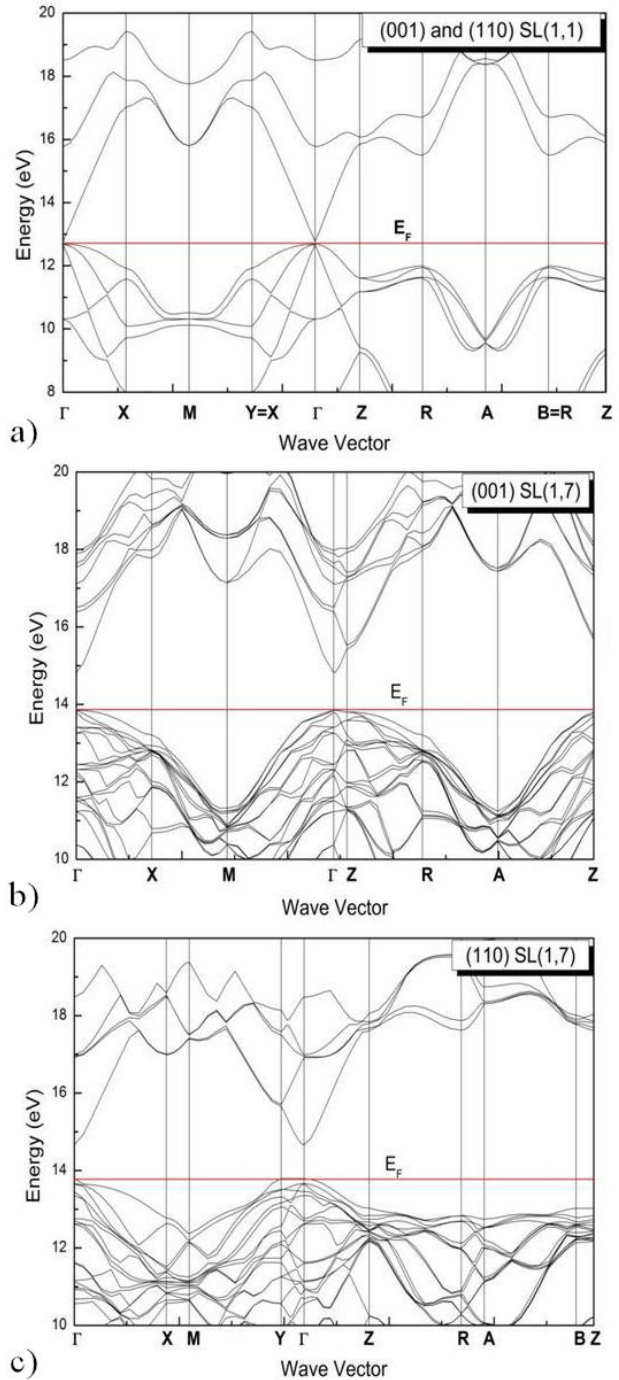


FIGURE 2. The band structure of superlattice $(\text{InN})/(\text{GaN})_n$ with $n = 1, 7$ for both (001) and (110) cases.

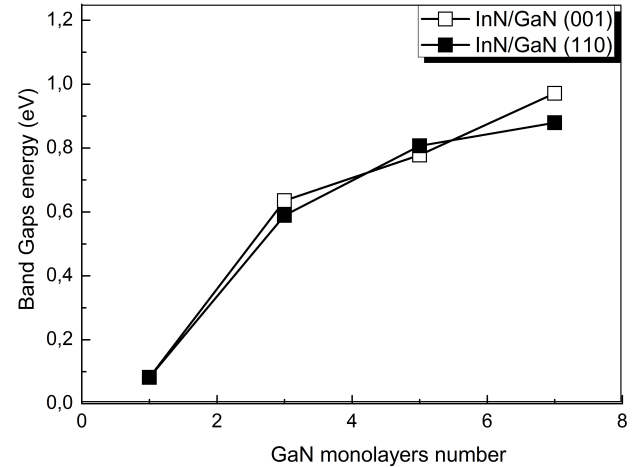
of CB at R and A becomes higher, and it is at Z for (001)- SL_s and Y for (110) SL_s that the bottom of CB starts to lower rapidly. This competition between different high symmetry points of the SL_s is mainly due to the zone folding effect, which is a typical feature for SL_s . In other words, BZ of bulk binaries are folded into a smaller zone in a SL_s . In fact, any wavefunction of the SL_s at any high symmetry point k_{SL} can be written as a linear combination of the wavefunctions

TABLE III. The gap energies (in eV) between the upper VB and the lower CB.

Gaps	Both (001) and (110) SL (1,1)	(001)-SL (1,3)	(001)-SL (1,5)	(001)-SL (1,7)	(001)-SL (1,3)	(110)-SL (1,5)	(110)-SL (1,7)
Γ - Γ	0.0819	0.635	0.777	0.971	0.589	0.677	0.879
Γ -X	4.339	3.532	4.0631	3.936	3.229	3.912	3.207
Γ -Y	Y does not exist in SL(1,1)	Like Γ -X	Like Γ -X	4.464	2.877	2.227	1.864
Γ -M	3.116	3.261	3.308	3.298	4.568	3.222	3.610
Γ -Z	3.169	2.222	1.738	1.577	3.464	3.829	3.823
Γ -R	2.809	4.276	3.698	4.136	3.472	3.741	3.838
Γ -B	B does not exist in SL(1,1)	Like Γ -R	Like Γ -R	Like Γ -R	3.885	3.731	3.985
Γ -A	5.687	4.323	3.811	3.589	5.317	4.819	4.520

of the bulk constituent materials at specific points k_B of the bulk. These points are linked to each other by the following formula: $k_B = k_{SL} \pm (0, 0, 1/(m+n)) \times 2\pi/a_0$ [51]. As the period of the SL_s increases along with k , the SL_s BZ volume decreases. This is due to the number of times the bulk energy bands have to be folded (twice, four, six, and eight times according to the value of n) in order to be contained within the SL_s BZ. For example, in the case of the $n = 1$, the bulk bands need only be folded in half. We should mention that the number of atoms contained in the $SL_s 2(m+n)$ is bigger than in bulk. It is for these reasons that the number of valence electrons contained within the SL_s unit cell is $2L$ times the number of atoms contained within the bulk unit cell, then there are $2L$ times more energy levels than in the bulk material [54]. Table III summarizes the results concerning the gaps obtained in our different samples.

In order to estimate the effect of n number of monolayers into $(\text{InN})/(\text{GaN})_n SL_s$ on energies band gaps, we have plotted in Fig. 3 the variations of the $\Gamma - \Gamma$ gap versus SL thickness in both directions (*i.e.*, versus the number n of monolayers). We remark that the $\Gamma - \Gamma$ gap increases with thickness from $n = 1$ to $n = 7$ by 0.889 eV and 0.797 eV for the two directions (001) and (110) respectively. We also notice that the $\Gamma - \Gamma$ gap in (001) differs by more than 92 meV from the (110)-oriented SL_s ; this can be understood by considering the orientation dependence of the ordering potential in the (110) direction, which is given by $2 \cdot (V_{\text{GaN}} - V_{\text{InN}})/n$ [55]. For a better understanding of the symmetry of the present SL_s , we advise the reader to look into the very pedagogical paper of Gopalan *et al.* [56]. By paying attention to the difference between these SL_s and bulk binaries in details, it is notably visible that the $\Gamma - \Gamma$ direct gap of SL_s is lower than the fundamental gaps of GaN $\Gamma - \Gamma$ and then is not obtained from the interpolation of their binaries. It is found that the energy band gap $\Gamma - \Gamma$ increases slowly with increasing barrier thickness from $n = 5$, converging to a value near the fundamental gaps of GaN. I. Gorczyca *et al.* [3] show that (i) the increase of the barrier width (above about 10 monolayers)

FIGURE 3. Direct band gap energies ($\Gamma - \Gamma$) as a function of the number n of monolayers in the superlattice $(\text{InN})/(\text{GaN})_n$ for both (001) and (110)-oriented SL_s .

seems to have negligible effect on band gap $\Gamma - \Gamma$ in the (001) case. Although, it can be seen that the bandgap increase slowly in the (110) than (001) due to the weaker confinement, which allows us to say that the number of monolayers n is bigger in the (110) case and (ii) the contributions to the InN well wave functions arriving from adjacent GaN layers cause a significant increase of the local gap from the value 0.7 eV (appertaining to bulk InN) to about 2.1 eV in the InN layer in these SL_s . Therefore, it appears that the band gaps are most sensitive to the good thickness than to the barrier breadth and that the dependence on barrier thickness is different for SL_s with a various number of good monolayers. Here, the fundamental gap of InN is very important because it reduces the quantum confinement effect in the SL_s .

Such quantum confinement effects will influence the $\Gamma - \Gamma$ bandgap values of these SL_s . According to Ref. [57], the conventional InN/GaN QW are found to be type I, signification that the band gap values of SL_s are controlled by the InN region, but the major challenges for this conventional system

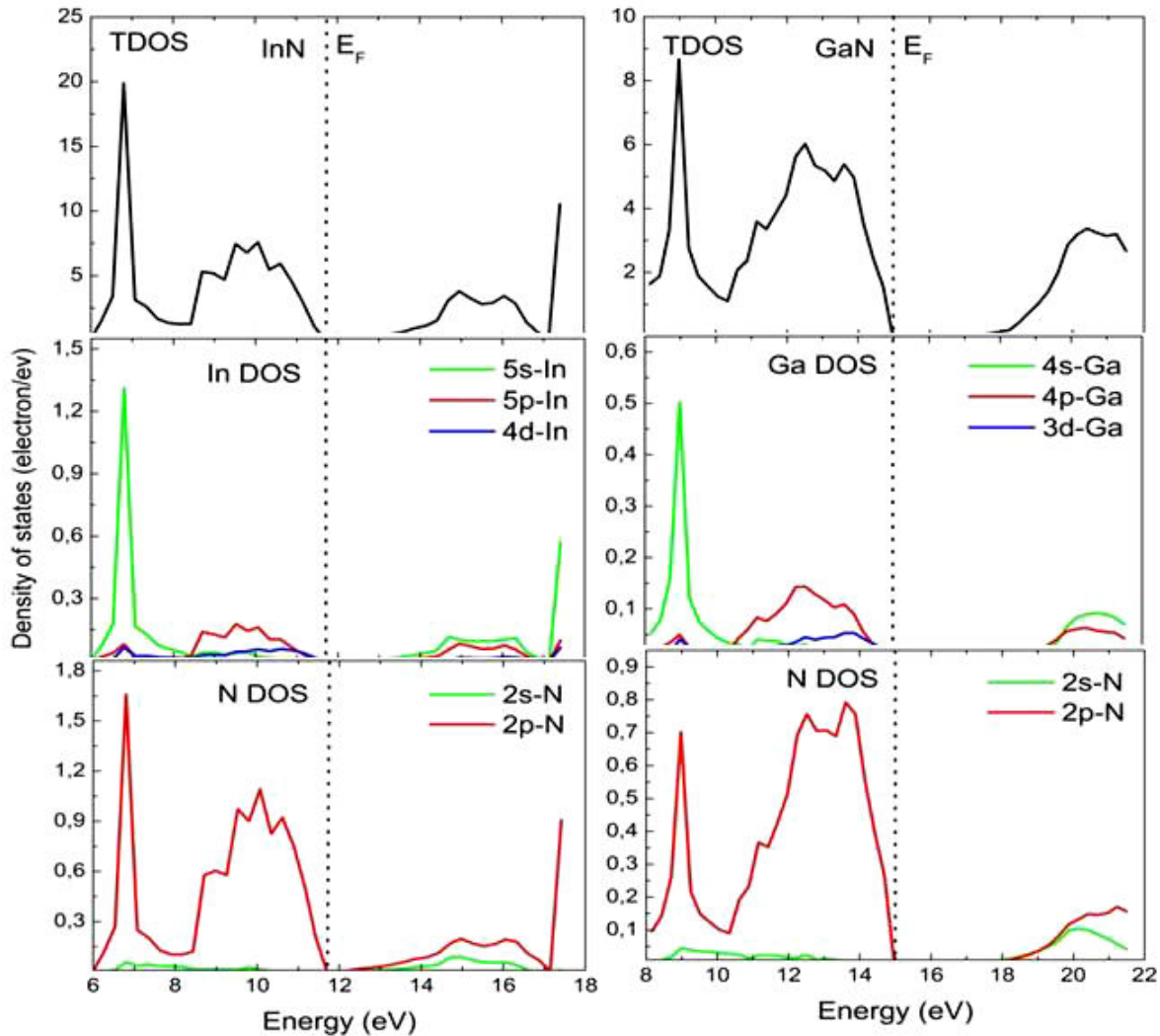


FIGURE 4. Total and partial density of states (DOS) for InN and GaN compounds.

are the largely spontaneous and piezoelectric polarization fields, which significantly reduce the optical gain of the SL_s . However, compared to the (001) case, the direction (110) is predicted to exhibit low quantum confinement effects, *i.e.*, there is a low built-in electric field in the well InN or barrier GaN regions. We can conclude that for a rationally period and low concentrations of In, these conventional systems are very good optical materials.

In the following, we want to comprise what happens in the two cases of SL_s by comparing directly the peaks of the different density of states (DOS) curves and by analyzing the partial densities as a function of different numbers of GaN monolayers in the SL_s . For reasons of comparison, the DOS of the bulk materials have been calculated. The VB of binaries was divided into low, intermediate, and high-energy subbands. In both InN and GaN, we have found that VB near the Fermi level E_f was mostly due to orbital p of In and N and orbital d of Ga and In atoms, while the greatest contribution to the bottom of CB was due to orbital p of N and s

of In for InN and orbital s of N and Ga and orbital p of N for GaN (Fig. 4). As an example, we show in Fig. 5 the total and partial density of states of two limit configurations ($n = 1$ and $n = 7$). The total and partial DOS profiles illustrate the participation in the electronic interactions of the orbitals and their positions. The first little peak, which occurs in the VB of (001) and (110) SL_s , shows a strong contribution from the s orbital of Ga atom. The following VB peaks are all due to a high mixing of orbitals p of the three atoms N, Ga and In and orbital d of Ga and In atoms. The CB peaks are all due to a high mixing of p , s , and d orbitals of N, Ga and In atoms for both (001) and (110)-oriented SL_s . We can see a little difference in the (110)- SL_s , where the contribution of the orbitals d of In atom and s of N atom decrease (increase) considerably from $n = 3$ to $n = 7$ in VB near E_f . It is clear from these results that the orbitals contribute almost similarly to the higher VB's and lower CB's in the (001) and (110)-oriented SL_s . The conclusion given in this section will be confirmed by the investigations of the optical properties reported below.

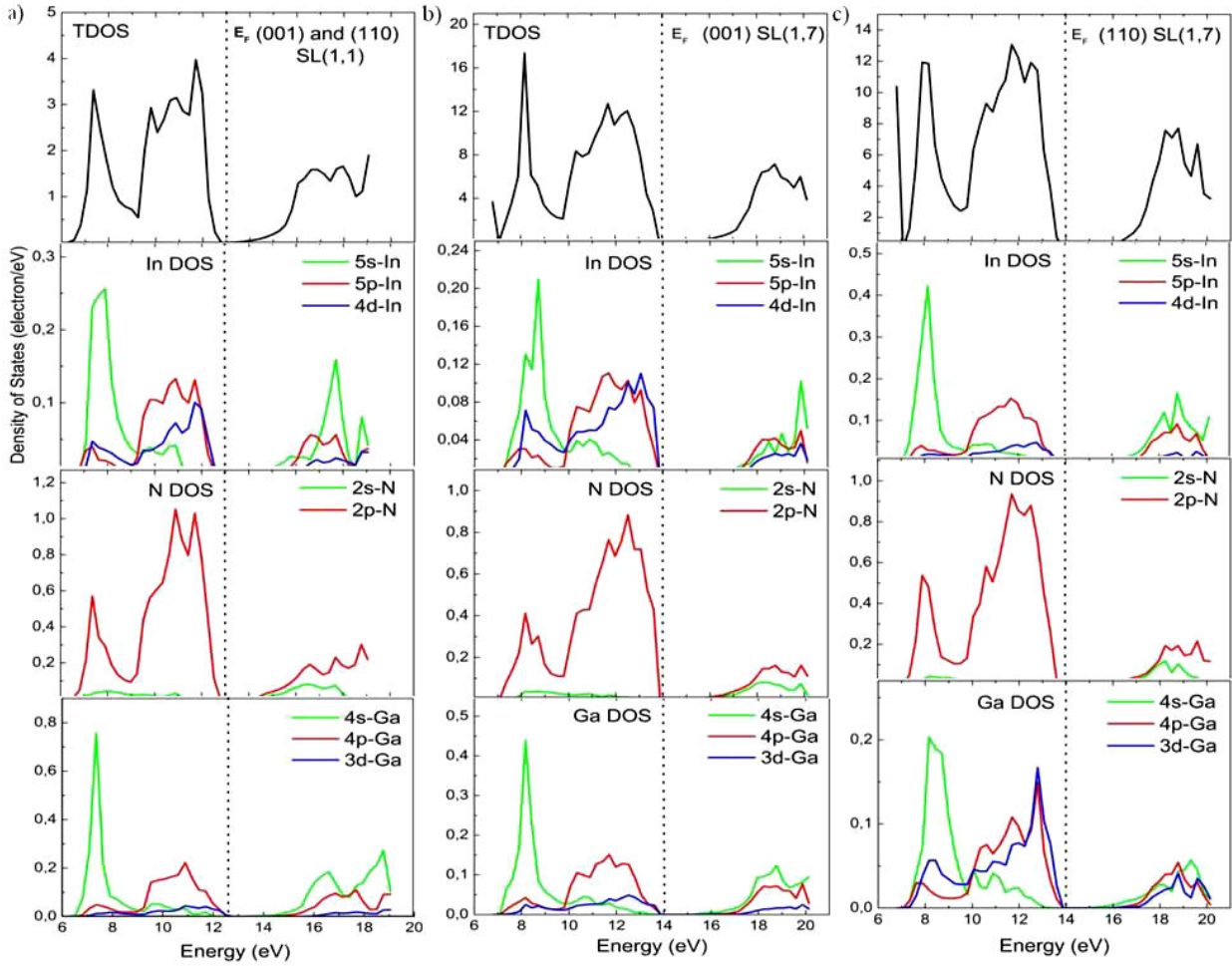


FIGURE 5. Total and partial density of states (DOS) for $(\text{InN})/(\text{GaN})_n$ of both (001) and (110) oriented SL_s ($n = 1$ and 7).

3.3. Optical Properties

It is fundamental to know to acquaint the optical activity of materials for their application in optoelectronic devices. In this consideration, we investigate the optical properties of both directions (001) and (110)-oriented SL_s for different monolayers n . These important properties may be attracted per the complex dielectric function $\varepsilon(\omega) = \varepsilon_1(\omega) + i \cdot \varepsilon_2(\omega)$, which is determined mostly by the transition between the valence and conduction bands. Where $\varepsilon_1(\omega)$ and $\varepsilon_2(\omega)$ are the real and imaginary parts of the dielectric function, respectively [58]. The imaginary part of the dielectric function, $\varepsilon_2(\omega)$ has been obtained directly from the momentum matrix elements between the occupied and the unoccupied wave functions [59]. The real part $\varepsilon_1(\omega)$ of the dielectric function can be derived from the imaginary part using the Kramers-Kronig relation [60]. Both real and imaginary parts allow the calculation of important optical functions such as refractive index $n(\omega)$ and absorption coefficient $\alpha(\omega)$ using the following relations [61].

$$n(\omega) = \left[\left(\varepsilon_1^2(\omega) + \varepsilon_2^2(\omega) \right)^{\frac{1}{2}} + \varepsilon_1(\omega) / 2 \right]^{\frac{1}{2}} \quad (4)$$

$$\alpha(\omega) = \frac{4\pi}{\lambda} / \lambda \cdot k(\omega) \quad (5)$$

Where k is the extinction coefficient, λ is the wavelength of light in the vacuum. To show all the possible optical transitions, we have increased the number of special points in the First BZ up to 600 k-points, with an energy range of up to 20 eV. Figure 6 shows the real and imaginary parts of the dielectric function for $SL(1,3)$, $SL(1,5)$, and $SL(1,7)$ compounds for both growth axis. The occurrence of the peaks in $\varepsilon_2(\omega)$ is principally produced through the inter-band or intra-band optical transitions. The contribution of intra-band transitions is important only in the case of metals [62]. $\varepsilon_2(\omega)$ spectra represented in terms of the optical transition between the filled and vacant states of various SL_s in both (001) and (110) cases are quite dissimilar and reflect various optical transitions. By increasing n , the peaks move to higher energy, which might be strongly dependent on the ionic polarization of the SL_s due to the large electronegativity of N. The curves of $\varepsilon_2(\omega)$ indicate that the threshold energy (first critical point) occurs at 0.665, 0.833, 0.998 eV in (001) case (0.605, 0.866, 0.899 eV in (110) case) for $n = 3, 5, 7$, respectively. These values correspond to the electronic transition value ($\Gamma_{V \rightarrow C}$).

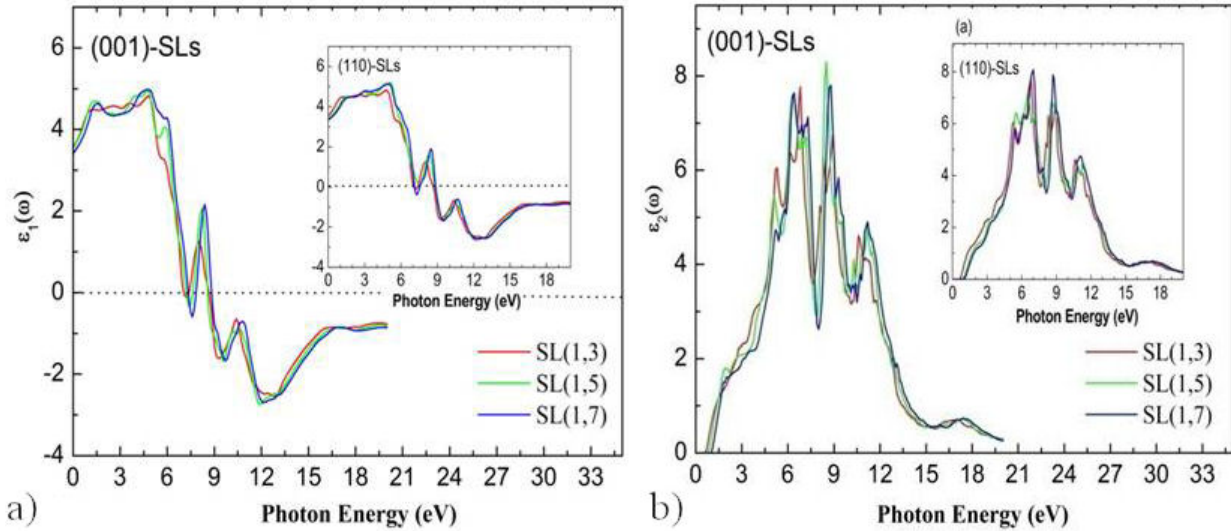


FIGURE 6. Calculated dielectric functions (real and imaginary parts) for $(\text{InN})/(\text{GaN})_n$ superlattices at direct band gap for the (001) growth axis direction. The inset of figure shows the real and imaginary parts plot for (110) growth axis direction.

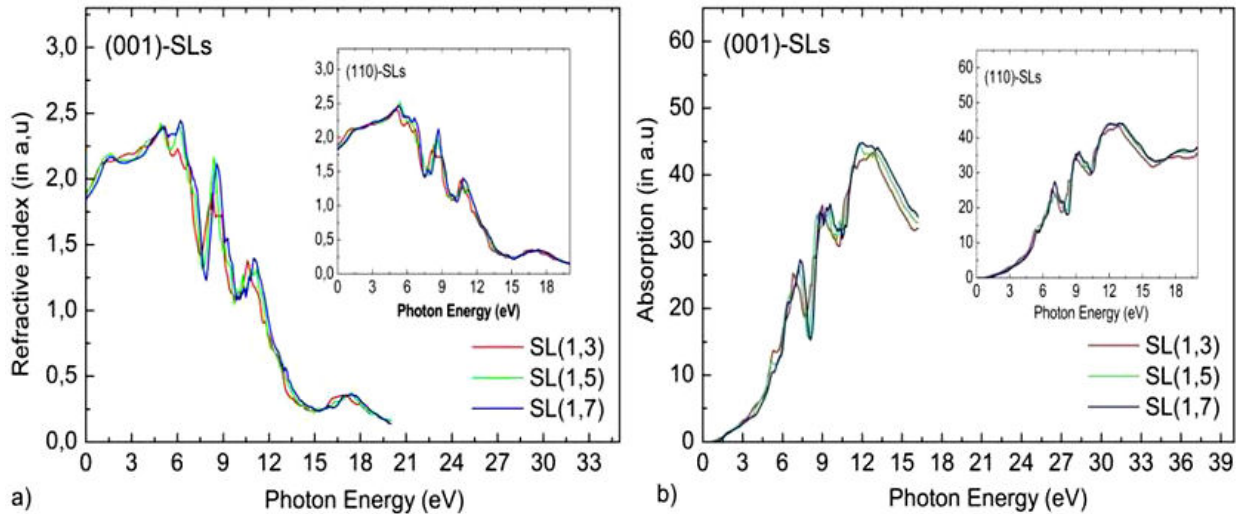


FIGURE 7. Calculated Refractive indices $n(\omega)$ (a) and absorption coefficients $\alpha(\omega)$ (b) for $(\text{InN})/(\text{GaN})_n$ superlattices for the (001) growth axis direction. The inset of figure shows the Refractive indices and absorption coefficients plot for (110) growth axis direction.

This point represents the fractionation $\Gamma_{V \rightarrow C}$, which gives the threshold of the direct optical transitions between the highest state of the valence band and the lowest state of the conduction band, which is identified as the fundamental absorption edge. Beyond these points, the curves increase rapidly. As a general observation, all curves of Fig. 6b show three major peaks in our calculations, appearing the resonance behavior. The maximum absorption for the three SL_s is situated at 6.80, 6.366, 8.799 eV in (001) case (6.766, 6.50, 7.01 in (110) case), respectively. Note that some changes in the edge or onset of the states are detected in the dielectric function plots in (110). This could be attributed to the difference between the optical transition states as well as the characteristic asymmetry in the electronic valence charge density distribution and in the bonding charge around the atoms. For both (001) and (110)-oriented SL_s , the most optical transi-

tions contribute to these peaks occur from occupied p orbital of Ga and N atoms and d orbital of Ga atom localized in the highest valence band to unoccupied s orbital of N, Ga, and In atoms localized in lowest conduction band.

The variation of the $\varepsilon_1(\omega)$ according to the energy for the SL_s is represented in Fig. 6a. We have noted that these optical spectrum represented in Fig. 6a are similar to small differences (The position and the height of peaks for both growth axes). The limiting value of the real part of the complex dielectric function obtained at a frequency of irradiation approaching zero is called static dielectric constant $\varepsilon_1(0)$. Our calculated values of $\varepsilon_1(\omega)(0)$ found in this way are summarized in Table IV. The calculated static dielectric constant $\varepsilon_1(0)$ decreases with increasing n monolayers, which is consistent with the decrease of the direct bandgap value, indicating that the is in an inverse relationship with bandgap ac-

TABLE IV. Calculated static optical constants $\varepsilon_1(0)$ and Static refractive index $n(0)$ for (InN)/(GaN) $_n$ Superlattice compounds.

(001)-oriented Superlattice		
Compounds	$\varepsilon_1(0)$	$n(0)$
SL(1,3)	3.502	1.871
SL(1,5)	3.490	1.868
SL(1,7)	3.396	1.842
(110)-oriented Superlattice		
Compounds	$\varepsilon_1(0)$	$n(0)$
SL(1,3)	3.553	1.885
SL(1,5)	3.365	1.834
SL(1,7)	3.312	1.820

corded to the Penn model [63]. We have concluded that the number of layers used effects the real parts of the dielectric functions for all configurations, and they have an important effect in the (110) case.

The refractive index of (InN)/(GaN) $_n$ SL_s is a valuable tool for the design of photovoltaic and optoelectronic devices. In order to study the transparency of SL_s in response of an incident light the relation of Eq. (3) is used for computed the theoretical refractive index values for all SL_s . The refraction spectra $n(x)$ and refractive index $n(0)$ are depicted in Fig. 7a and reported in Table IV. For the calculated SL_s $n(x)$ is not presenting a large variation for the photon energy in the near infrared or visible radiation. As a result, the static refractive indices $n(0)$ are estimated from the refraction spectra (see Table IV). The maximum refractive index is reached for photon energy around 5.0, 4.89, 6.23 eV for (001) case (5.10, 5.40, 5.30 eV for (110) case), respectively. The spectral plots of the refractive index of Fig. 7a show an increasing from 2.424 (for $n = 3$) to 2.449 (for $n = 7$) in the (001) SL_s , and its value increases from 2.424 (for $n = 3$) to 2.457 (for $n = 7$) for (110)-oriented SL_s . According to the result in both directions, the influence of the indium composition in the refractive index values of SL_s are more important for (001) direction compared to the (110) direction, which allows us to say that the refractive index of SL_s depends on growths axes.

The optical absorption spectra are calculated in order to distinguish the optical nature in the SL_s . The dispersion in the optical absorption spectra of the $SL(1, n)$ grown along both directions ($n = 3, 5, 7$) are plotted in Fig. 7b. The absorption peak of both directions shifts to higher energy when n increases and the threshold energy increases. We observe from the curves of Fig. 7b that the absorption edge begins

from the energy values of 0.600, 0.833, and 1.0 eV for (001) case (0.600, 0.766 and 0.9 eV for (110) case), respectively. It shifts towards lower energy when compared to bulk GaN, whose threshold is located at $E_s = 2.05$ eV. Two major peaks at approximately 7 eV and 8.9 eV in the absorption coefficient for both growth axes represent the absorption of light at two different wavelengths. The maximum value of $\alpha(\omega)$ is approximately 12.5 eV for (001) case (12.8 eV for (110) case) for all values of n , then the absorption coefficient abruptly decreases for the light photon above these energies. The intensity of absorption spectra diminishes with the inclusion of In contents in GaN layers.

As a result, the main conclusion to retain from all these curves is that the growth direction (110) does not ameliorate the optical activity. The similar contribution of the atomic orbitals to the electronic properties is probably the main reason for which the optical properties are expected not to be modified significantly. We suppose that the contribution of great cells will not change the present conclusions, on account of increasing the cell will only make the contribution of the bulk important compared to that of the interface and may not ameliorate the optical activity anymore.

4. Conclusion

To sum up we presented an ab-initio calculation on the electronic and optical features of short-period (InN)/(GaN) $_n$ superlattice systems, with n varying between 1 and 7, within both directions (001) and (110) using the FPLMTO+GGA96 method, which allows an accurate treatment of the interstitial regions. For the electronic proprieties, these (110) systems have a semiconductor behavior with variable energy gaps values. It is also observed that the band structure of all superlattices possesses a direct bandgap. Furthermore, the calculated dielectric functions, refractive index, and absorption spectra of the (001) SL_s tend not to be quite different from those of (110) SL_s . The reason is the slight differences between the contribution of the atomic orbitals to the electronic properties in both directions. The investigations were not extended to large systems because the contribution of the orbitals to electronic properties may reproduce, and the same conclusions should hold.

Acknowledgements

The authors are thankful to the DGRSDT for the provided support to accomplish this research. This work has been supported by Applied Materials Laboratory (A.M.L).

1. N. Mehnane, N. Oukli, and M. Ouki, *Chin. J. Phys.* **55** (2017) 1275, <https://doi.org/10.1016/j.cjph.2017.06.004>
2. A. Laref, A. Altujar, S. Laref, and S.J. Luo, *Sol. Energy*. **142** (2017) 231, <https://doi.org/10.1016/j.solener.2016.12.009>
3. I. Gorczyca, T. Suski, N. E. Christensen, and A. Svane, *Cryst. Growth Des.* **12** (2012) 3521. <https://doi.org/10.1021/cg300315r>
4. M. Oukli, N. Mehnane, N. Oukli, B. Bachir Bouiadjra, and H. Belghoul, *Phys. E* **114** (2019) 113653, <https://doi.org/10.1016/j.physe.2019.113653>
5. P. Strak, P. Kempisty, K. Sakowski, and S. Krukowski, *J. Cryst. Growth*. **401** (2014) 652, <https://doi.org/10.1016/j.jcrysgro.2014.01.069>
6. A. Assali *et al.*, *Mater. Sci. Semicond. Process.* **36** (2015) 192, <https://doi.org/10.1016/j.mssp.2015.03.033>
7. I. Gorczyca, T. Suski, N. E. Christensen, and A. Svane, *J. Phys: Condens. Matter*. **30** (2018) 063001, <https://doi.org/10.1088/1361-648X/aaa2ae>
8. I. Gorczyca *et al.*, *Jpn. J. Appl. Phys.* **52** (2013) 08JL06. <https://doi.org/10.7567/JJAP.52.08JL06>
9. D. Eric, J. Jiang, A. Imran, M. N. Zahid, and A. A. Khan, *Results Phys.* **13** (2019) 102246. <https://doi.org/10.1016/j.rinp.2019.102246>
10. Y. Li, B. Liu, R. Zhang, Z. Xie, and Y. Zheng, *Phys. E* **44** (2012) 821. <https://doi.org/10.1016/j.physe.2011.12.014>
11. K. Matsuoka, S. Yagi, and H. Yaguchi, *J. Cryst. Growth*. **477** (2017) 201. <https://doi.org/10.1016/j.jcrysgro.2017.05.021>
12. Z. Touaa and N. Sekkal, *Acta Cryst. B* **68** (2012) 378. <https://doi.org/10.1107/S0108768112030091>
13. A. Bhuiyan, K. Sugita, A. Hashimoto, and A. Yamamoto, *IEEE J. Photovolt.* **2** (2012) 276. DOI: 10.1109/JPHOTOV.2012.2193384
14. T. Suski *et al.*, *Appl. Phys. Lett.* **104** (2014) 182103. <https://doi.org/10.1063/1.4875558>
15. A. Duff, L. Lymparakis, and J. Neugebauer, *Phys. Status Solidi. B* **252** (2015) 855. <https://doi.org/10.1002/pssb.201451687>
16. M. Oukli, N. Mehnane, and H. Abid, *Chin. J. Phys.* **54** (2016) 60. <https://doi.org/10.1016/j.cjph.2016.03.004>
17. Y. Cherchab, B. Amrani, N. Sekkal, M. Ghezali, and K. Talbi, *Phys. E* **40** (2008) 606. <https://doi.org/10.1016/j.physe.2007.08.122>
18. F. Tair, N. Sekkal, B. Amrani, W. Adli, and L. Boudaoud, *Superlattices Microstruct.* **41** (2007) 44. <https://doi.org/10.1016/j.spmi.2006.11.002>
19. N. E. Christensen and I. Gorczyca, *Phys. Rev. B* **44** (1991) 1707. <https://doi.org/10.1103/PhysRevB.44.1707>
20. F. Szmulowicz, H. J. Haugan, and G. J. Brown, Quantum Sensing and Nanophotonic Devices V, *Proc. of SPIE* **6900** (2008) 69000L. <https://doi.org/10.1117/12.763738>
21. K. C. Hall *et al.*, *Phys. Rev. B* **68** (2003) 115311. <https://doi.org/10.1103/PhysRevB.68.115311>
22. H. Fritzsche, M. Saoudi, Z. Yamani, W. J. L. Buyers, R. A. Cowley, and R. C. C. Ward, *Phys. Rev. B* **77** (2008) 054423. <https://doi.org/10.1103/PhysRevB.77.054423>
23. M. Sawicki, G. J. Bowden, P. A. J. de Groot, B. D. Rainford, and J. M. L. Beaujour, *Appl. Phys. Lett.* **77** (2000) 573. <https://doi.org/10.1063/1.127048>
24. G. P. Dimitrakopoulos *et al.*, *J. Appl. Phys.* **123** (2018) 024304. <https://doi.org/10.1063/1.5009060>
25. F. Szmulowicz, H. J. Haugan and G. J. Brown, *J. Appl. Phys.* **104** (2008) 074505. <https://doi.org/10.1063/1.2990003>
26. G. F. Karavaev, V. N. Chernyshov, and R. M. Egunov, *Semiconductors*. **37** (2003) 573. <https://doi.org/10.1134/1.1575364>
27. H. Xia, Y. Feng, R. Patterson, X. Jia, S. Shrestha, and G. Conibeer, *J. Appl. Phys.* **113** (2013) 164304. <https://doi.org/10.1063/1.4802683>
28. Alistair T. Meney, *Superlattices and Microstructures*. **77** (1992) 31. [https://doi.org/10.1016/0749-6036\(92\)90358-C](https://doi.org/10.1016/0749-6036(92)90358-C)
29. I. Gorczyca, K. Skrobas, T. Suski, N. E. Christensen, and A. Svane, *J. Appl. Phys.* **114** (2013) 223102. <https://doi.org/10.1063/1.4843015>
30. G. Staszczak *et al.*, *J. Appl. Phys.* **113** (2013) 123101. <https://doi.org/10.1063/1.4796101>
31. S. Y. Savrasov, *Phys. Rev. B* **54** (1996) 16470. <https://doi.org/10.1103/PhysRevB.54.16470>
32. J. P. Perdew, S. Burke, and M. Ernzerhof, *Phys. Rev. Lett.* **77** (1996) 3865. <https://doi.org/10.1103/PhysRevLett.77.3865>
33. M. Merabet *et al.*, *Chin. J. Phys* **60** (2019) 462. <https://doi.org/10.1016/j.cjph.2019.05.026>
34. J. P. Perdew and Y. Wang, *Phys. Rev. B* **45** (1992) 13244. <https://doi.org/10.1103/PhysRevB.45.13244>
35. F. D. Murnaghan, *Proc. Natl. Acad. Sci. USA*. **30** (1944) 5390. doi: 10.1073/pnas.30.9.244
36. I. Vurgaftman, and J. R. Meyer, *J. Appl. Phys.* **94** (2003) 3675. <https://doi.org/10.1063/1.1600519>
37. Bo-Ting Liou, *Jpn. J. Appl. Phys.* **47** (2008) 3350. <https://doi.org/10.1143/JJAP.47.3350>
38. B. Amina, A. Lachebi, A. Shuhaimi, S. A. Rahman, and H. Abid, *Optik* **127** (2016) 11577. <https://doi.org/10.1016/j.ijleo.2016.09.014>
39. M. I. Ziane, Z. Bensaad, T. Ouahrani, and H. Bennacer, *Mater. Sci. Semicond. Process.* **30** (2015) 181. <https://doi.org/10.1016/j.mssp.2014.08.039>
40. S.-g. Zhu, J.-j. Shi, S. Zhang, M. Yang, Z.-q. Bao, and M. Zhang, *Appl. Phys. B* **104** (2011) 105. <https://doi.org/10.1007/s00340-011-4473-8>

41. M. E. Sherwin, and T. J. Drumond, *J. Appl. Phys.* **69** (1991) 8423. <https://doi.org/10.1063/1.347412>
42. Z. Boussahla, B. Abbar, B. Bouhafs, and A. Tadjer, *J. Solid State Chem.* **178** (2005) 2117. <https://doi.org/10.1016/j.jssc.2005.03.047>
43. P. Rinke, M. Winkelnkemper, A. Qteish, D. Bimberg, J. Neugebauer, and M. Scheffler, *Phys. Rev. B.* **77** (2008) 075202. <https://doi.org/10.1103/PhysRevB.77.075202>
44. M. J. Espitia R, O. S. Parra, and C. O. López, *J. Magn. Magn. Mater.* **451** (2018) 295. <https://doi.org/10.1016/j.jmmm.2017.11.070>
45. H. Achour, S. Louhibi-Fasla, and F. Mana, *Phys. Procedia.* **55** (2014) 17. <https://doi.org/10.1016/j.phpro.2014.07.003>
46. S. P. Tamariz-Kaufmann, A. A. Valladares, A. Valladares, and R.M. Valladares, *J. Non-Cryst. Solids.* **420** (2015) 7. <https://doi.org/10.1016/j.jnoncrysol.2015.03.037>
47. J. Serrano, A. Rubio, E. Hernández, A. Muñoz, and A. Mujica, *Phys. Rev. B* **62** (2000) 16612. <https://doi.org/10.1103/PhysRevB.62.16612>
48. M. I. Ziane, Z. Bensaad, T. Ouahrani, B. Labdelli, and H. Abid, *Mater. Sci. Semicond. Process.* **16** (2013) 1138. <https://doi.org/10.1016/j.mssp.2013.02.016>
49. H. Baaziz, Z. Charifi, A. H. Reshak, B. Hamad, and Y. Al-Douri, *Appl. Phys. A* **106** (2012) 687. <https://doi.org/10.1007/s00339-011-6666-8>
50. S. Saib, and N. Bouarissa, *Phys. B* **387** (2007) 377. <https://doi.org/10.1016/j.physb.2006.04.023>
51. K. Talbi, Y. Cherchab, and N. Sekkal, *Eur. Phys. J. Appl. Phys.* **58** (2012) 30103. <https://doi.org/10.1051/epjap/2012110307>
52. R. Ahmed, H. Akbarzadeh, and F. e-Aleem, *Phys. B* **370** (2005) 52. <https://doi.org/10.1016/j.physb.2005.08.044>
53. L.K. Teles, and L.M.R. Scolfaro, *Appl. Phys. Lett.* **80** (2002) 1177. <https://doi.org/10.1063/1.1450261>
54. D. J. Wolford, T. F. Keuch, and J. A. Bradley, *Phys. Rev. B* **35** (1987) 1196. <https://doi.org/10.1103/PhysRevB.35.1196>
55. S. Froyen, D. M. Wood, and A. Zunger, *Appl. Phys. Lett.* **54** (1989) 2435. <https://doi.org/10.1063/1.101100>
56. S. Gopalan, N. E. Christensen, and M. Cardona, *Phys. Rev. B* **39** (1989) 5165. <https://doi.org/10.1103/PhysRevB.39.5165>
57. R. A. Arif, H. Zhao, and N. Tansu, *Appl. Phys. Lett.* **92**, (2008) 011104, <https://doi.org/10.1063/1.2829600>.
58. S. Adachi, *Properties of Semiconductor Alloys: Group-IV, III-V and II-VI Semiconductors*, Edit, John Wiley and Sons, Ltd., (2009), DOI:10.1002/9780470744383
59. D. Allali *et al.*, *Phys. B* **443** (2014) 24, <https://doi.org/10.1016/j.physb.2014.02.053>.
60. P. Y. Yu, and M. Cardona, *Fundamentals of Semiconductors: Physics and Materials Properties*, 4th edn. (Springer, Berlin, 2010), <https://doi.org/10.1007/978-3-642-00710-1>.
61. V. Antonov, B. Harmon, and A. Yaresko, *Electronic Structure and Magneto-Optical Properties of Solids*, 1st edn. (Kluwer Academic Publishers, New York, 2004), <https://doi.org/10.1007/1-4020-1906-8>
62. M. Merabet *et al.*, *Physica B* **406** (2011) 3247, <https://doi.org/10.1016/j.physb.2011.05.034>.
63. D. R. Penn, *Phys. Rev* **128** (1962) 2093, <https://doi.org/10.1103/PhysRev.128.2093>.